# Description of soft tissue artifacts and related consequences on hindlimb kinematics during canine gait

Cheng-Chung Lin[1], Shi-Nuan Wang[2], Ming Lu[2], Tzu-Yi Chao[2], Tung-Wu Lu[3] and Ching-Ho Wu[2,4]

[1] Department of Electrical Engineering, Fu Jen Catholic University, New Taipei City, Taiwan
[2] Institute of Veterinary Clinical Science, National Taiwan University, Taipei, Taiwan
[3] Department of Biomedical Engineering, National Taiwan University, Taipei, Taiwan
[4] Department of Surgery, National Taiwan University Veterinary Hospital, Taipei, Taiwan

## ABSTRACT

**Background:** Soft tissue artifacts (STAs) are a source of error in marker-based gait analysis in dogs. While some studies have revealed the existence of STAs in the canine hindlimb, STAs and their influence on kinematic gait analysis remain unclear.
**Methods:** Thirteen healthy Taiwan dogs affixed with twenty skin markers on the thigh and crus were recruited. Soft tissue artifacts and their influence on the determination of segment poses and stifle angles were assessed by simultaneously measuring marker trajectories and kinematics of the underlying bones via a model-based fluoroscopic analysis method.
**Results:** Markers on the thigh showed higher STAs than those on the crus, with root-mean-square amplitudes up to 15.5 mm. None of the tested marker clusters were able to accurately reproduce the skeletal poses, in which the maximum root-mean-square deviations ranged from 3.4° to 8.1°. The use of markers resulted in overestimated stifle flexion during 40–60% of the gait cycle and underestimated stifle flexion during 80–90% of the gait cycle.
**Conclusions:** Considerable magnitudes and effects of STAs on the marker-based 3D gait analysis of dogs were demonstrated. The results indicate that the development of error-compensation techniques based on knowledge regarding STAs is warranted for more accurate gait analysis.

Submitted 15 January 2020
Accepted 28 May 2020
Published 26 June 2020

Corresponding author
Ching-Ho Wu,
chinghowu@ntu.edu.tw

Academic editor
Robert Druzinsky

Additional Information and Declarations can be found on page 17

DOI **10.7717/peerj.9379**



**Subjects** Animal Behavior, Veterinary Medicine, Zoology, Kinesiology, Orthopedics
**Keywords** Fluoroscopy, Gait analysis, Kinematics, Marker, Soft tissue artifacts, Locomotion

## INTRODUCTION

Skin marker-based motion capture has been widely applied for measuring canine gait kinematics in three-dimensional (3D) or two-dimensional (2D) space (*Carlisle et al., 2019*; *Fu, Torres & Budsberg, 2010*; *Kim, Rietdyk & Breur, 2008*; *Torres et al., 2015*), yielding quantitative information regarding the biomechanics of the joints in normal and abnormal states (*Bockstahler et al., 2012*; *Carlisle et al., 2019*; *Lorke et al., 2017*; *Sanchez-Bustinduy et al., 2010*). However, it is acknowledged that markers attached to the skin surface become displaced with respect to the underlying skeleton along with movement of the body (*Leardini et al., 2005*). Such skin marker movement results in "soft tissue artifacts"

(STAs) or "skin movement artifacts" that diminish the accuracy of the reconstructed motion variables and are difficult to eliminate with common mathematical filters.

According to the STAs of individual markers attached to the limbs, clusters formed by markers on a segment were found to translate and rotate with respect to the underlying bone and deform from their original shape during body exercise (*De Rosario et al., 2012*; *Grimpampi et al., 2014*), leading to error in the measured segment poses and the calculated joint kinematics (*Lin et al., 2016*). Regarding human motion analysis, STA-related studies have quantified the amplitudes, patterns and influence of STAs (*Akbarshahi et al., 2010*; *Barré et al., 2015*; *Hume et al., 2018*; *Kuo et al., 2011*; *Li et al., 2012*; *Tsai et al., 2011*) and explored the hidden factors that affect them (*Clément et al., 2018*; *Li et al., 2017*; *Lin et al., 2016*). It is generally accepted that STAs are considered subject-, location- and task-specific (*Leardini et al., 2005*; *Peters et al., 2010*). In particular, distinct motion tasks with inconsistent ranges of joint motion have been shown to lead to different STA magnitudes for individual markers (*Akbarshahi et al., 2010*; *Tsai et al., 2009*), which further differently affect the calculated segment and knee kinematics (*Akbarshahi et al., 2010*; *Benoit, Damsgaard & Andersen, 2015*; *Li et al., 2012*; *Peters et al., 2010*; *Stagni et al., 2005*). Even under well-controlled coherent motion, loading conditions that affect the activities of the underlying muscles can cause the magnitudes of the STAs to vary (*Li et al., 2017*). Physical characteristics of the body, such as obesity, age and total knee replacement, have also been reported to influence STAs and their impacts on the description of knee kinematics (*Clément et al., 2018*; *Lin et al., 2016*). Considering the conspicuous differences in body shape and gait characteristics between species, there is no direct evidence that the STA patterns from the human lower limb during gait can accurately reflect marker movements in the canine hindlimb. In the context of human STAs, the modeling of STAs (*Bonci et al., 2014*; *Dumas & Jacquelin, 2017*) and error-compensation approaches, such as single-body optimization (*Chèze, Fregly & Dimnet, 1995*), multibody kinematics optimization with joint constraints (*Lu & O'Connor, 1999*; *Richard, Cappozzo & Dumas, 2017*) and calibration procedures (*Cappello et al., 2005*), have been proposed in an attempt to improve the accuracy of marker-based motion analysis.

In canine gait analysis, STAs were first revealed and characterized by deformation of the calculated segment length during the gait due to the resulting skin movement (*Kim et al., 2011*; *Schwencke et al., 2012*). To assess the STA of individual markers, fluoroscopic analysis was conducted to quantify the planar displacement of radiopaque markers over anatomical bony landmarks (*Schwencke et al., 2012*). To determine 3D marker-level STAs, STA-free marker trajectories as a reference are required and can be reconstructed from the known kinematics of bones. Model-based fluoroscopy analysis integrating real-time fluoroscopy and computed tomography (CT) are viable methods for reproducing the kinematics of canine hindlimb segments (*Fischer, Lehmann & Andrada, 2018*; *Jones et al., 2014*; *Kim et al., 2015*). With a similar approach, the 3D displacement patterns of skin markers on the thigh and crus of dogs during isolated, passive stifle motion have been derived (*Lin et al., 2018a*). Rigid and nonrigid cluster-level STAs and various combinations

**Table 1** Canine subject signalment.

| Subject No. | Sex | Age (year) | Weight (kg) | Body condition score |
|---|---|---|---|---|
| 1 | F | 6 | 23 | 6 |
| 2 | F | 3 | 22 | 4 |
| 3 | F | 2 | 15 | 5 |
| 4 | F | 2 | 20 | 4 |
| 5 | F | 3 | 15 | 4 |
| 6 | F | 2 | 24 | 5 |
| 7 | F | 3 | 15 | 4 |
| 8 | M | 3 | 15 | 4 |
| 9 | M | 3 | 19 | 5 |
| 10 | F | 3 | 21 | 5 |
| 11 | M | 6 | 22 | 5 |
| 12 | M | 4 | 16 | 4 |
| 13 | M | 3 | 23 | 5 |
| Average | n/a | 3.3 | 19.2 | 4.6 |

of clusters in determining canine stifle joint angles have also been quantified (*Lu et al., 2020*).

Previous studies have demonstrated the existence of STAs during voluntary gait in dogs (*Kim et al., 2011*; *Schwencke et al., 2012*), and others have explored the magnitudes and patterns of marker-level (*Lin et al., 2018a*) and cluster-level STAs (*Lu et al., 2020*) based on the kinematics data of passive and isolated stifle flexion movement. However, during dynamic ambulation, which combines multiple joint motions, muscle contractions and inertial effects, the behavior of STAs and how the STAs affect the kinematic analysis of canine hindlimbs are unclear. No study has yet reported the STAs of individual markers and their related effects on computed stifle angles during canine gait. Therefore, this study aimed to assess the STAs of markers on the thigh and crus during voluntary gait activity in dogs and to quantify their influence on determining the poses of body segments and on the errors of the computed stifle joint angles.

## MATERIALS AND METHODS

### Dogs

Thirteen client-owned, adult Taiwan dogs (age: 3.3 ± 1.3 years; weight: 19.2 ± 3.6 kg; body condition score (BCS): 4.6/9, Table 1) were recruited for the study. No discernible abnormalities were detected on orthopedic or hindlimb radiographic examination, which was conducted by two experienced veterinary surgeons (CHW and SNW). BCS is a visual and palpated assessment of the amount of fat covering the bones of a dog regardless of body size (*Laflamme, 1997*); it was set to be within 4 to 6 in the present study to exclude enrolling over- or underconditioned dogs. The study was approved by the National Taiwan University's Institutional Animal Care and Use Committee (No: NTU106-EL-00221) and the University Hospital's Clinical Trial/Research Committee (Approval No: 000041).

Owners were informed of the experiment content and provided written informed consent prior to the experiment. Notably, the dogs enrolled in the study were all different from those in our previous related studies (*Lin et al., 2018a*; *Lu et al., 2020*).

## Bone model reconstruction

Computed tomography (Activion 16, Toshiba Medical Systems Corporation, Tochigi, Japan) images of the pelvic limbs of each dog completely covering the pelvis and right femur, tibia, fibula and foot bones were obtained with a voxel size of 0.625 mm × 0.625 mm × 0.3 mm. Contours of the femur and tibia were semimanually identified on all CT slices with the seeded region growing algorithm (*Rafael & Gonzalez, 2017*). Hounsfield unit values of voxels exterior to the segmented boundaries were set to −1,000. The volumetric bone model was obtained by extracting a sub-volume from the processed CT volume containing the target bone (Fig. 1E) (*Lin et al., 2018b*). A polygon-meshed surface model of the bone (Fig. 1E) was also generated based on the segmented contours using the marching cube algorithm (*Lorensen & Cline, 1987*). Bone-embedded anatomical frames were determined for the femur ($AF_{fe}$) and tibia ($AF_{ti}$) (Fig. 1F). Sites of anatomical landmarks and the determination of anatomical axes were described in *Fu, Torres & Budsberg (2010)*. The origin of the $AF_{fe}$ was defined at the midpoint of the femoral epicondyles, and that for the $AF_{ti}$ was defined at the proximal tibial crest. The 3D coordinates of the landmarks were manually identified from the surface models of the respective bones. All data processing for model reconstruction was performed using self-developed software implemented in MATLAB with the Image Processing Toolbox (MATLAB, 2017b; The Mathworks Inc., Natick, MA, USA).

## Motion acquisition

Twenty spherical, infrared-reflective markers with a diameter of 8 mm were attached to the skin surface of the right hindlimb of each dog, including 11 markers on the thigh and 9 on the crus, as shown in Fig. 1A. Detailed descriptions of the marker locations are provided in Table 2. Hair was first clipped locally to facilitate marker attachment; the markers were attached by one veterinary surgeon (SNW) using cyanoacrylate and an over-layer of adhesive tape. During marking and marker attachment, the dogs were kept awake and standing still on the ground.

Prior to motion data acquisition, a C-arm fluoroscopy system with a 30-cm-diameter image intensifier (Arcadis Avantic; Siemens Healthineers, Munich, Germany), a nine-camera motion capture system consisting of 6 Bonita B10 and 3 Vero cameras (Vicon Motion Systems Inc., Oxford, UK) and a dog treadmill (PetRun PR720F, Iwate International Developing Co., Ltd., Taiwan) were set up in an X-ray-shielded surgical room (Fig. 1B). Intrinsic parameters describing the fluoroscopic projection model and the fluoroscopic reference frame ($RF_f$) were determined through a calibration procedure using images of a custom-made calibration object (*Baltzopoulos, 1995*). Extrinsic parameters describing the transformation between the $RF_f$ and the reference frame provided by the motion capture system were obtained by spatially registering the coordinates of six designated markers in two reference frames (*Lin et al., 2018a*).

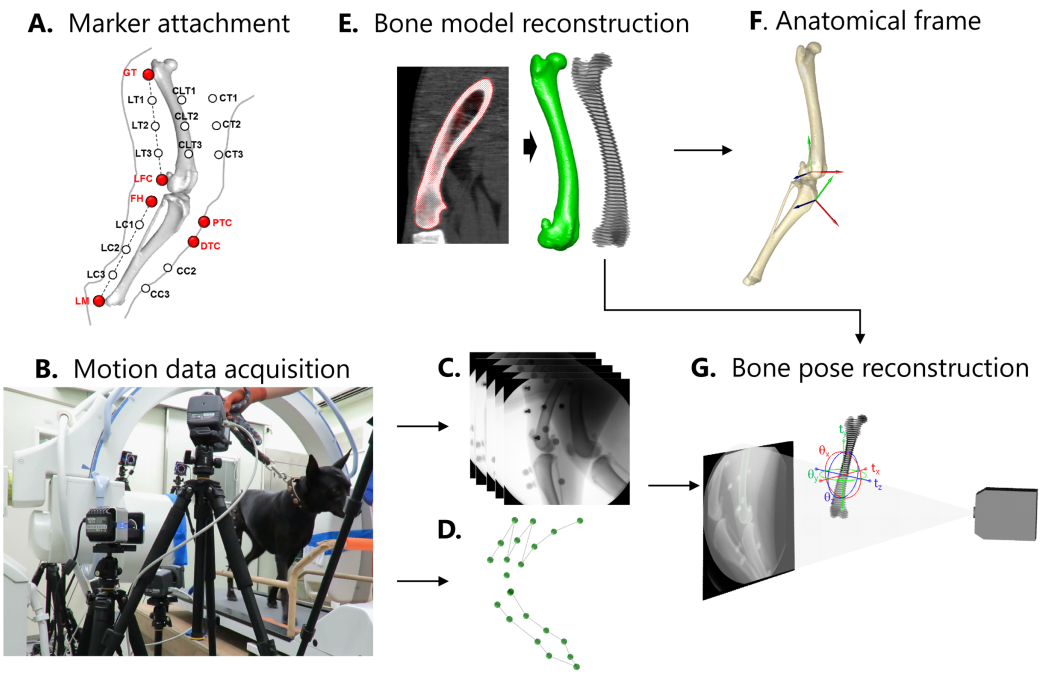


**Figure 1 Procedures for motion data acquisition and reconstruction.** (A) A total of twenty markers were attached to each dog's right hindlimb. Six markers were placed on anatomical landmarks, namely, the greater trochanter (GT), lateral femoral condyle (LFC), fibular head (FH), proximal and distal tibial crests (PTC and DTC) and lateral malleolus (LM). The others were evenly distributed on the cranial and lateral skin surfaces of the thigh and crus. Three lateral thigh markers (LT1-3) were evenly distributed between the GT and LFC. The cranial thigh markers (CT1-3) were attached to cranial surfaces at a height equal to that of the lateral markers while the subject was standing still. The craniolateral thigh markers (CLT1-3) were placed between the cranial and lateral markers. The crus marker locations were designed in a similar manner, except for the craniolateral and cranioproximal markers, given that the tibia and regions were occupied by the anatomical landmark markers. (B) After the markers were attached, the dogs were then instructed to walk on the treadmill while the fluoroscopy system and motion capture system were operated to collect (C) X-ray fluoroscopic images and (D) marker trajectories. (E) The dogs also underwent CT imaging to obtain subject-specific image volumes, which were then processed, segmented and reconstructed to generate computerized bone models. (F) With the surface bone models, anatomical frames of the femur and tibia were determined. (G) Three-dimensional skeletal poses were reconstructed using a model-based fluoroscopy analysis method.

Full-size DOI: 10.7717/peerj.9379/fig-1

The dog was then instructed to walk on the treadmill at a speed of 2.5 kph (~0.7 m/s) in a natural cadence (Fig. 1B). The speed was set according to the results of previous studies (*Piazza et al., 2017*) and to avoid the blurring of fluoroscopic images. Fluoroscopy was operated in digital cine mode (tube voltage: 53.4 ± 0.9 kVp; tube current: 27.2 ± 2.9 mA) to collect mediolateral fluoroscopic images at a frame rate of 30 fps and a resolution of 1024 × 1024 pixels (Fig. 1C). Meanwhile, the motion capture system was operated at 120 fps to acquire skin marker trajectories (Fig. 1D). Overall, three successful trials involving at least three full gait cycles (GCs) for each trial were collected. For each trial, a full GC with better image quality compared with multiple other GCs was manually chosen for subsequent analysis. All dogs were trained for three sessions in a month to adapt to walking on the treadmill prior to motion capture. In addition, subject calibration was

**Table 2 Marker locations on the canine hindlimb for soft tissue artifact analysis.** The * symbol represents markers attached to anatomical landmarks.

| Segment | Marker | Description |
|---|---|---|
| Thigh | GT* | Greater trochanter (anatomical landmark) |
| | LFC* | Lateral femoral condyle (anatomical landmark) |
| | LT1 | The marker attached to the lateral thigh and located ~25% down the line from the GT to the LFC |
| | LT2 | The marker attached to the lateral thigh and located in the middle between the GT and the LFC |
| | LT3 | The marker attached to the lateral thigh and located ~75% down the line from the GT to the LFC |
| | CT1 | The marker attached to the cranial aspect of the thigh at the same height as LT1 in the standing posture |
| | CT2 | The marker attached to the cranial aspect of the thigh at the same height as LT2 in the standing posture |
| | CT3 | The marker attached to the cranial aspect of the thigh at the same height as LT3 in the standing posture |
| | CLT1 | The marker attached to the craniolateral aspect of the thigh and located in the middle between CT1 and LT1 |
| | CLT2 | The marker attached to the craniolateral aspect of the thigh and located in the middle between CT2 and LT2 |
| | CLT3 | The marker attached to the craniolateral aspect of the thigh and located in the middle between CT3 and LT3 |
| Crus | FH* | Head of the fibula (anatomical landmark) |
| | LM* | Lateral malleolus (anatomical landmark) |
| | PTC* | Proximal tibial crest (anatomical landmark) |
| | DTC* | Distal tibial crest (anatomical landmark) |
| | LC1 | The marker attached to the lateral crus and located ~25% down the line from the FH to the LM |
| | LC2 | The marker attached to the lateral crus and located in the middle between the FH and the LM |
| | LC3 | The marker attached to the lateral crus and located at ~75% down the line from the FH to the LM |
| | CC2 | The marker attached to the cranial aspect of the crus at the same height as LC2 in standing posture |
| | CC3 | The marker attached to the cranial aspect of the crus at the same height as LC3 in standing posture |

performed to acquire images and marker data when the dog stood still on the inactive treadmill.

## Reconstruction of stifle kinematics

The 3D positions and orientations (i.e., 3D poses) of the femur and tibia were reproduced by best matching the corresponding volumetric bone models to the single-plane fluoroscopic images using a 3D/2D image registration method (*Lin et al., 2013*). Image registration was automatically conducted frame-by-frame for images over a full GC using self-developed software (Fig. 1G) (*Lin et al., 2018b*; *Lin et al., 2013*), and the whole process was repeated three times. The 3D positions and orientations obtained from the multiple image registrations ($n$ = 3) were averaged to give the final estimation of bone pose. A preliminary study was conducted to assess the accuracy of the image registration based on a cadaveric canine hindlimb during simulated gait. The mean absolute errors of the determined bone poses were less than 0.38 mm for the in-plane translations, 1.62 mm for the out-of-plane translations and 0.53° for all rotations.

Motion analysis software (Nexus; Vicon Motion Systems Inc., Oxford, UK) was used to preprocess and label the marker trajectories, which were then exported and expressed in $RF_f$ after the coordinate transformation with extrinsic parameters. At the subject calibration trial, given the reproduced bone poses from model-based fluoroscopy analysis,

position vector of each marker with respect to the AF of the underlying bone was derived and denoted as "local marker" in the current study (*Lin et al., 2018a*). Following the 4-marker cluster convention (*Cappozzo et al., 1997*), any four arbitrary local markers on one segment can constitute a cluster template. The marker-determined 3D pose of a segment was determined using a pose estimator by best registering the cluster template to the measured skin markers (*Söderkvist & Wedin, 1993*). Due to the existence of STAs, the marker-determined poses of body segments may not coincide with the bone-determined poses. Given the 3D segment poses, the stifle joint angles were calculated as the rotation of the crus with respect to the thigh and are expressed in Cardan angles using a *z-x-y* sequence (*Wu & Cavanagh, 1995*), giving the joint angles in the sagittal plane (flexion/extension, Flex/Ext), dorsal plane (internal/external rotation, I/E rotation) and transverse plane (adduction/abduction, Add/Abd).

## STA analysis

To assess marker-level STAs, the position vectors of all the markers in the corresponding AF were obtained given the bone-determined segment poses for each instant during the GC. The position vector of a marker can vary during gait owing to soft tissue deformation; thus, the mean position vector was determined over the full GC. For each marker at each instant, the total displacement amplitude and the amplitude components along the cranial/caudal (C/C), proximal/distal (P/D) and lateral/medial (L/M) axes were obtained by subtracting the mean vector from its position vector. The root-mean-square amplitude (rmsa) across the $N$ instants during a full GC were analyzed, indicating the levels of the STAs for the markers (*Cereatti et al., 2017*). In addition, peak-to-peak amplitude, $\Delta p_{\max}$, and the amplitude components along the C/C, P/D and L/M axes, $\Delta p_c$ ($c$ = C/C, P/D and L/M), were also quantified to represent the maximum variation of marker displacement (*Cereatti et al., 2017*).

To assess the influence of STAs on canine gait analysis, errors in the marker-determined segmented poses and joint kinematics were quantified. Three different marker cluster compositions were chosen for assessment. The first cluster (M1) consisted mainly of markers on anatomical landmarks, including the greater trochanter (GT) and lateral femoral condyle (LFC) of the femur and fibular head (FH), proximal and distal tibial crests (PTC and DTC) and lateral malleolus (LM) of the tibia/fibula. Two additional markers at the cranial aspect of the thigh (CT1 and CT3) were included to comply with the 4-marker convention and avoid collinearly aligning markers that shared the highest isotropic index value (*Cappozzo et al., 1997*). The isotropic index, defined as the ratio of the two prevailing axes of the distribution of the markers, was computed to quantify the level of collinearity among the markers. The smaller the isotropic indices were, the more collinear the markers. A minimum isotropic index of 0.5 was suggested for the marker compositions, as the collinear markers are insufficient for estimating orientation with the pose estimator (*Cappozzo et al., 1997*). The second cluster (M2) consisted of the suggested set of markers with the smallest rigid cluster-level STAs during isolated stifle motion (*Lu et al., 2020*). The third (M3) consisted of markers with isotropic indices greater than 0.5 and with the smallest cumulative marker-level STAs found in the current study.

With the chosen cluster templates (M1, M2, and M3), the corresponding marker-determined segment poses and joint angles were calculated. All kinematic variables at every 1% of the normalized GC from paw contact (0%) to the next paw contact (100%) were obtained by piecewise cubic interpolation and then averaged across three trials for individual dogs. We then quantified the orientation deviations of the marker-determined segment poses with respect to the bone-determined poses during the GC. Orientation deviations are expressed in terms of L/M tilt about the C/C axis, I/E rotation about the P/D axis and C/C tilt about the L/M axis of a body segment. Root-mean-square deviations (rmsds) over the stance phase, swing phase and the full GC were assessed. Marker-determined and bone-determined stifle Flex/Ext, I/E rotation and Abd/Add were compared by paired *t*-test with a significance level of 0.05, and their differences were assessed with the rmsd. All numerical and statistical analyses were performed using MATLAB (MATLAB 2017b; The Mathworks Inc., Natick, MA, USA).

## RESULTS

The cranial thigh markers (CT1-3) had greater STAs than the craniolateral and lateral thigh markers during the GC, for which the averaged rmsa and $\Delta p_{\max}$ reached 15.5 mm and 47.9 mm, respectively. Proximal/distal displacement was the primary STA component for the cranial thigh markers, while C/C displacement was mainly found for the lateral thigh markers, including those of the GT and LFC. The craniolateral thigh markers (CLT1-3) exhibited similar STA patterns to those of CT1-3 but with a smaller error amplitude in the P/D direction (Figs. 2 and 3). The crus markers had lower STAs, for which the averaged rmsa and $\Delta p_{\max}$ were less than 5.3 mm and 18.2 mm, respectively. The P/D rmsa, ranging from 3.5 mm to 4.7 mm, was the primary error component for the FH, PTC and LC1 and the most prominent STA on the crus (Fig. 2). The averaged rmsa values in the L/M direction were below 4.1 mm for the thigh markers and 1.4 mm for the crus markers (Fig. 2).

During the stance phase, the stifle flexion angles varied from 38.7° to 49.7°, during which the cranial thigh markers were displaced proximally and the laterodistal markers (LT2, LT3, and LFC) exhibited cranial displacement (Fig. 4B). The GT marker exhibited displacement opposite to that of the laterodistal markers (Fig. 4B). The crus markers closer to the stifle joint were also displaced proximally in the stance phase, while the others moved in inconsistent directions with magnitudes below 4.3 mm (Fig. 4C). In the swing phase, stifle flexion increased and reached a maximum angle of 80.3° near the middle of the period (77% GC) (Fig. 4A). During 60–80% GC, the markers generally moved in directions opposite to those during the stance phase with slightly greater displacement (Figs. 4D and 4E). During the terminal swing, the markers gradually returned to their original locations by the next paw contact (0%).

The marker compositions of clusters M2 and M3 on the crus were found to be identical (Table 3). For any of the tested marker clusters (M1, M2, and M3), the estimated C/C tilt and I/E rotation of the femur were considerably affected by STAs, for which the rmsd ranged from 5.4° to 8.1° (Table 4). The rmsds in the L/M tilt were below 2.2° (Table 4). Cranial tilts were observed during 0–20% and 75–100% GC, while caudal tilts were

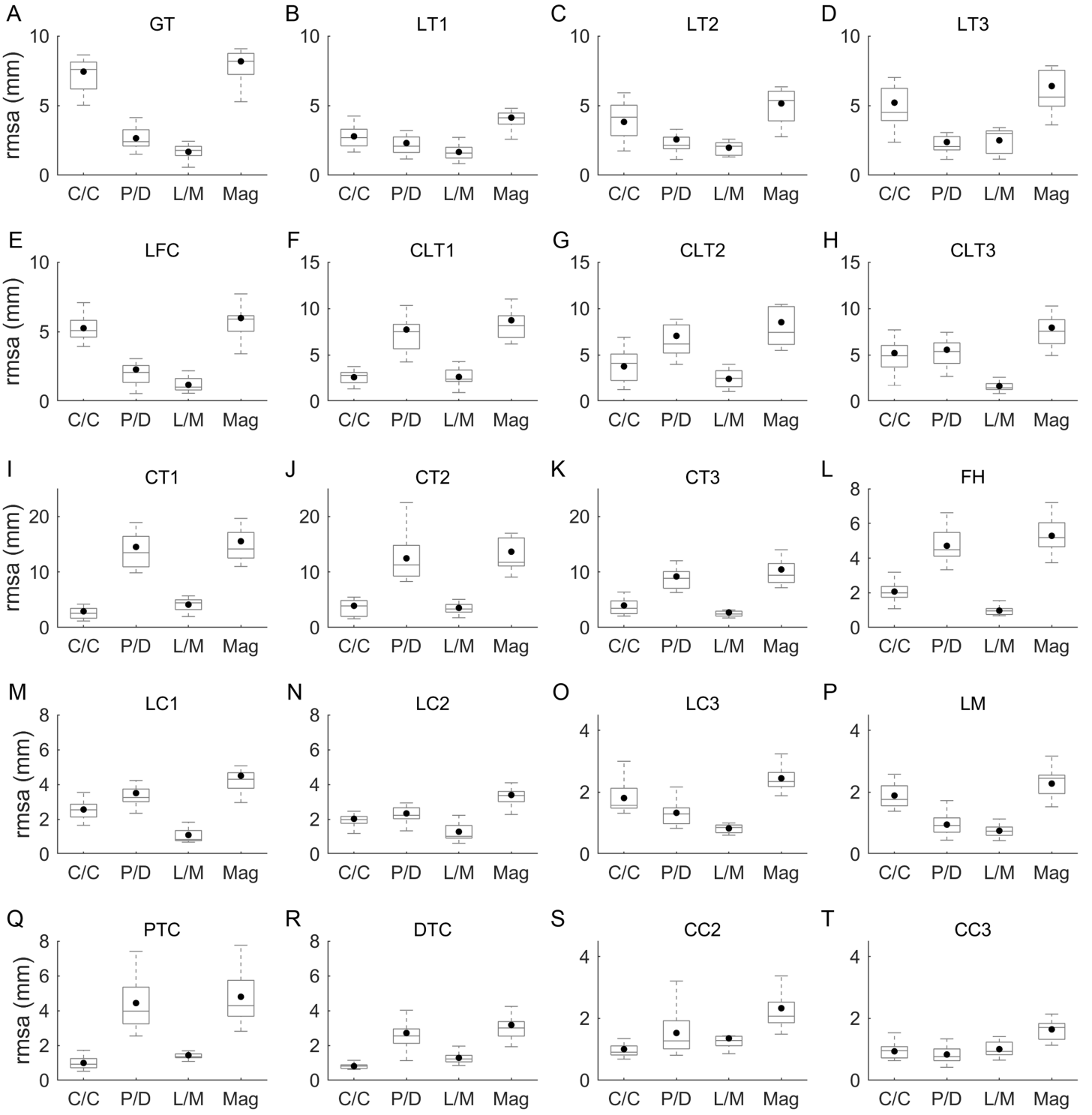


**Figure 2 Boxplot of the root-mean-square amplitude (rmsa) of the marker displacement errors across all dogs (A–T).** The central lines and dots indicate the median and mean values, respectively. The top and bottom sides of the box represent the 75th and 25th percentiles of the error distribution, respectively, and the whiskers indicate the extreme values. Outliers are not shown. Full-size DOI: 10.7717/peerj.9379/fig-2

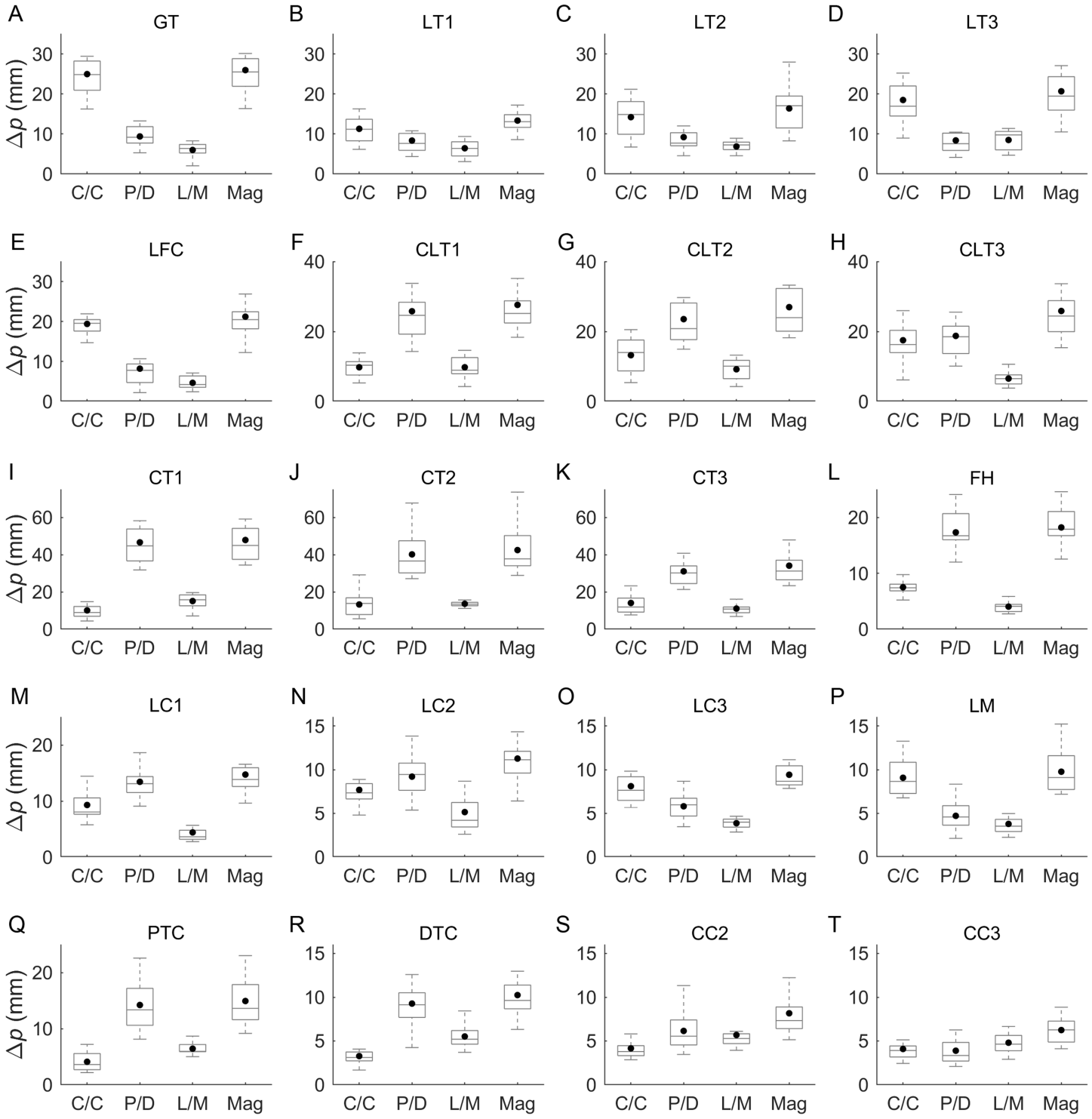


**Figure 3 Boxplot of the peak-to-peak amplitude of the marker displacement errors across all dogs (A–T).** The central lines and dots indicate the median and mean values, respectively. The top and bottom sides of the box represent the 75th and 25th percentiles of the error distribution, respectively, and the whiskers indicate the extreme values. Outliers are not shown. Full-size DOI: 10.7717/peerj.9379/fig-3

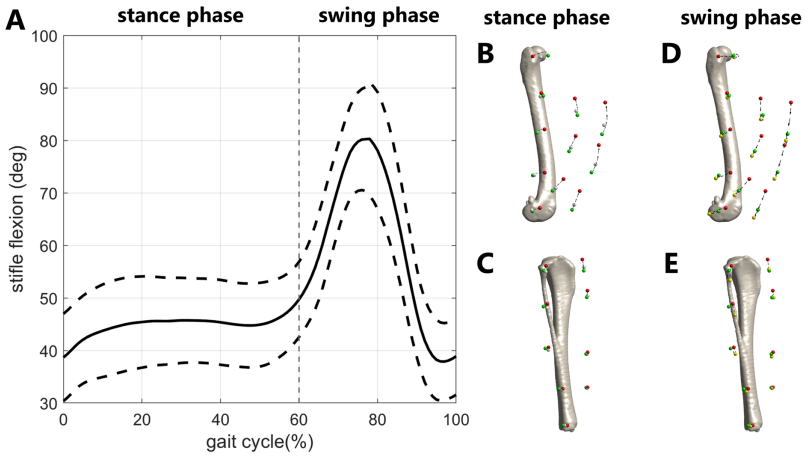


**Figure 4 Soft tissue artifact patterns on the thigh and crus during the gait cycle.** (A) The means (black solid lines) and standard deviations (black dashed lines) of the stifle flexion angles of the right hindlimb during a complete stride. (B and C) In the stance phase, the average displacement of the skin markers from paw contact (0%, green) to paw off (60%, red) are displayed. The white spheres indicate the original marker locations measured during subject calibration, with the dog standing still. (D and E) In the swing phase, the average displacements of the markers from paw off (60%, red) and mid-swing (80%, yellow) to the next paw contact (100%, green) are displayed. Full-size DOI: 10.7717/peerj.9379/fig-4

**Table 3 Marker compositions of the cluster used for kinematics analysis.**

| Marker cluster composition | Thigh | Crus |
|---|---|---|
| Marker cluster #1 (M1) | GT, LFC, CT1, CT3 | FH, LM, PTC, DTC |
| Marker cluster #2 (M2) | LT1, LT2, CT2, LFC | LC2, LC3, CC2, CC3 |
| Marker cluster #3 (M3) | LT1, LT2, CLT1, CLT2 | LC2, LC3, CC2, CC3 |

observed during 40–70% GC (Fig. 5C). The use of M1 and M3 resulted in an averaged I/E rotation deviation of the femur up to approximately 5°, with relatively high between-subject variability (Fig. 5B). The marker STAs showed slightly less of an influence on the estimated tibial orientation, in which I/E rotation, with an rmsd up to 4.6°, was the most affected component (Table 4). Although considerable between-subjects variability was present, the marker-determined orientations for the crus showed an averaged external rotation of 4° with respect to the bone-determined poses using the M2 cluster near the paw strike period (0–10% and 90–100% GC) (Fig. 5E).

The marker-determined stifle kinematics deviated from the bone-determined kinematics, for which the maximum rmsds were 8.7°, 6.1° and 7.2° for Flex/Ext, Add/Abd and I/E rotation, respectively (Table 4). The marker-determined stifle flexion angles were significantly higher during 40–60% GC (mean differences ≤ 13°) and lower during 80–90% GC (mean differences ≤9.9°), with slight differences among the tested clusters (Table 5). Significant differences between the marker-determined and bone-determined angles were found in the transverse and dorsal planes, with mean differences up to 5.0° and 5.7°, respectively, and the STA had different influences among the tested clusters (Table 5).

**Table 4** Root-mean-square deviations of segment and stifle kinematics.

| | Study | Stance phase (0–60%) | | | Swing phase (60–100%) | | | Full gait cycle (0–100%) | | |
|---|---|---|---|---|---|---|---|---|---|---|
| | | **Femur** | | | | | | | | |
| | | **L/M tilt** | **I/E Rot.** | **C/C tilt** | **L/M tilt** | **I/E Rot.** | **C/C tilt** | **L/M tilt** | **I/E Rot.** | **C/C tilt** |
| rmsd | M1 | 1.2 (0.7) | 5.9 (2.0) | 5.6 (1.8) | 1.4 (0.8) | 5.6 (2.7) | 5.7 (2.5) | 1.3 (0.7) | 5.9 (2.2) | 5.7 (2.0) |
| | M2 | 1.9 (0.9) | 6.4 (2.8) | 5.3 (2.0) | 1.8 (0.8) | 5.8 (2.7) | 5.5 (2.5) | 1.9 (0.8) | 6.3 (2.5) | 5.4 (2.0) |
| | M3 | 1.9 (0.7) | 6.8 (3.5) | 8.2 (1.9) | 2.6 (1.1) | 7.2 (2.9) | 7.9 (3.0) | 2.2 (0.8) | 7.1 (3.1) | 8.1 (2.2) |
| | *Barre et al. (2013)* | 1.0 (0.6) | 4.0 (2.3) | 1.3 (0.5) | 1.2 (0.6) | 4.4 (2.3) | 3.9 (1.4) | n/a | n/a | n/a |
| | | **Tibia** | | | | | | | | |
| | | **L/M tilt** | **I/E Rot.** | **C/C tilt** | **L/M tilt** | **I/E Rot.** | **C/C tilt** | **L/M tilt** | **I/E Rot.** | **C/C tilt** |
| rmsd | M1 | 0.6 (0.2) | 3.3 (1.5) | 1.4 (1.1) | 0.7 (0.2) | 3.4 (1.2) | 1.7 (1.1) | 0.7 (0.2) | 3.4 (1.3) | 1.5 (1.1) |
| | M2/M3 | 1.8 (1.1) | 4.4 (1.8) | 1.6 (0.7) | 2.1 (1.2) | 4.8 (1.6) | 1.8 (0.8) | 2.0 (1.1) | 4.6 (1.7) | 1.7 (0.7) |
| | *Barre et al. (2013)* | 0.4 (0.2) | 1.2 (0.6) | 0.6 (0.3) | 0.7 (0.2) | 1.9 (0.7) | 1.0 (0.3) | n/a | n/a | n/a |
| | | **Stifle joint** | | | | | | | | |
| | | **Flex/Ext** | **Add/Abd** | **I/E Rot.** | **Flex/Ext** | **Add/Abd** | **I/E Rot.** | **Flex/Ext** | **Add/Abd** | **I/E Rot.** |
| rmsd | M1 | 6.1 (2.6) | 4.4 (1.9) | 5.0 (1.2) | 6.7 (3.4) | 4.4 (3.0) | 4.4 (1.3) | 6.4 (2.8) | 4.5 (2.4) | 4.8 (1.2) |
| | M2 | 5.9 (2.8) | 4.6 (2.4) | 7.2 (4.0) | 6.4 (3.2) | 4.9 (2.3) | 7.0 (2.4) | 6.2 (2.8) | 4.8 (2.2) | 7.2 (3.2) |
| | M3 | 8.8 (2.5) | 5.6 (3.7) | 6.6 (2.9) | 8.4 (3.8) | 6.5 (2.6) | 6.7 (2.3) | 8.7 (2.8) | 6.1 (3.1) | 6.7 (2.5) |
| | *Richard, Cappozzo & Dumas (2017)* | n/a | n/a | n/a | n/a | n/a | n/a | 2.9 | 2.7 | 2.1 |
| | *Barre et al. (2013)* | 1.6 (0.5) | 1.4 (0.7) | 3.9 (2.0) | 4.1 (1.4) | 3.0 (1.7) | 3.8 (1.4) | n/a | n/a | n/a |
| | *Akbarshahi et al. (2010)* | n/a | n/a | n/a | n/a | n/a | n/a | 4.5 | 4.45 | 5.91 |
| | *Reinschmidt et al. (1997)* | 2.1 (0.9) | 2.4 (0.4) | 3.9 (1.6) | n/a | n/a | n/a | n/a | n/a | n/a |

**Note**:
Means (standard deviations) of the root-mean-square deviations (rmsds) of the femoral and tibial orientations and stifle joint kinematics obtained by comparing the marker-determined and bone-determined kinematic variables. The values reported in the literature are also presented for comparison.

## DISCUSSION

The study first documented the amplitudes and patterns of STAs of markers on the thigh and crus and their influence on the estimation of segment 3D poses and stifle kinematics during canine ambulation via in vivo, 3D measurements. To faithfully reveal gait-induced STAs, we trained the dogs to walk on the treadmill prior to motion acquisition to increase the consistency of the gait characteristics and thus the STA patterns. In addition, multiple walking trials were performed for each subject, and the resulting STA outcomes were averaged over three trials to further diminish the within-subject variability of the STA quantities.

Directly comparing the marker STA magnitudes to those reported in our preceding study (*Lin et al., 2018a*) was difficult, as STA is considered subject- and task-specific (*Leardini et al., 2005*). In particular, prominent differences in the range of flexion angles can be found between the current and preceding studies owing to the different executed motion tasks (38.7–80.3° during gait and 32.4–124.3° during passive stifle motion). The hip and tarsal joint movements that involved during gait activities (*Torres et al., 2013*) were also largely restricted in our preceding studies (*Lin et al., 2018a*; *Lu et al., 2020*). However, a comparison of the major STA components and distributions found in the two studies on medium-sized dogs showed that the marker STA on the cranial aspect of the

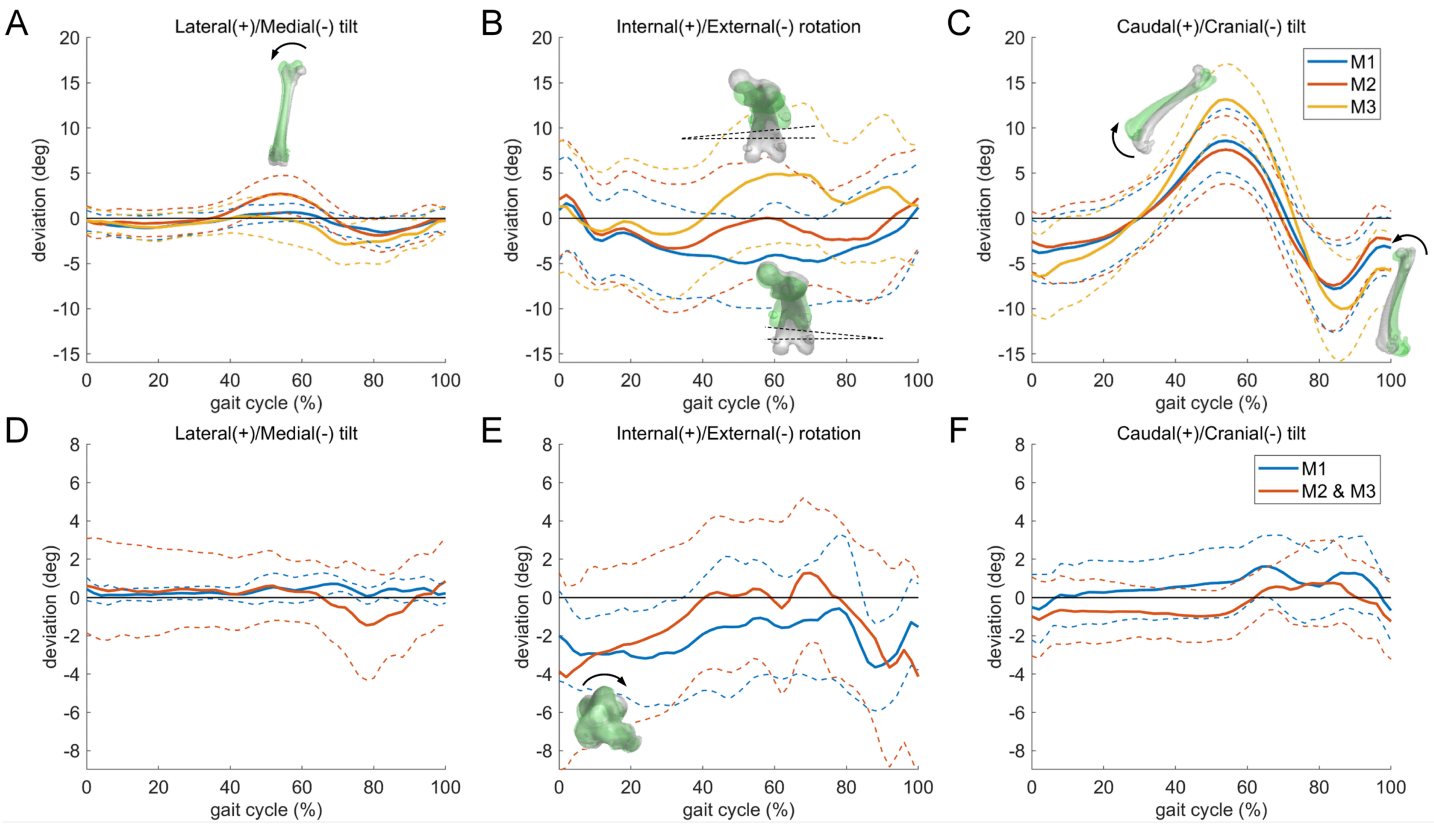


**Figure 5 Orientation deviations determined by skin markers with respect to the bone-determined poses.** (A–C) Means (solid lines) and standard deviations (dashed lines) of the femoral orientation deviation angles with respect to the bone-determined poses using the three tested marker clusters (M1: blue lines; M2: red lines; M3: yellow lines). (D–F) Means (solid lines) and standard deviations (dashed lines) of the tibial orientation deviation angles determined using the M1 (blue lines) and the M2 and M3 clusters (red lines). Note that the M2 and M3 clusters on the crus are composed of the same markers.
Full-size DOI: 10.7717/peerj.9379/fig-5

thigh exhibited the largest amplitude and was distributed mainly in the P/D direction (Figs. 2–4). Both studies showed that the C/C displacement was the most prominent STA component for the lateral thigh markers, including those of the GT and LFC (Figs. 2–4). These STA patterns were also similar to those found in human gait (*Akbarshahi et al., 2010*; *Tsai et al., 2009*). In comparison with the thigh markers, the crus markers, which were displaced with an average rmsa of less than 5.3 mm, appeared to be less influenced by the STA, in agreement with previous studies on dogs during passive flexion (*Lin et al., 2018a*) and on human gait (*Akbarshahi et al., 2010*; *Barré et al., 2015*; *Barre et al., 2013*; *Tsai et al., 2009*). The current findings, with a max. averaged rmsa of the thigh markers of up to 15.5 mm, which was clearly higher than that of the crus markers, showed an association with the circumference of the respective segments (*Smith et al., 2013*), indicating that the extent of soft tissue coverage may be one of the determinants of STAs in the canine hindlimb. This result was also demonstrated in another study conducted on sheep (*Taylor et al., 2005*).

During initial paw contact, the CT1-3 and CLT1-3 markers were normally displaced distally relative to the locations in subject calibration (Fig. 4B), which would tilt the

**Table 5** Influences of soft tissue artifacts on the calculated stifle angles with three tested marker clusters.

| Gait cycle (%) | Flexion/extension (°) | | | | Adduction/abduction (°) | | | | Internal/External Rotation (°) | | | |
|---|---|---|---|---|---|---|---|---|---|---|---|---|
| | Bone-det. | M1 | M2 | M3 | Bone-det. | M1 | M2 | M3 | Bone-det. | M1 | M2 | M3 |
| 0 | 38.7 ± 8.3 | 36.3 ± 9.6* | 36.5 ± 8.0 | 33.1 ± 8.5* | 4.7 ± 3.6 | 5.5 ± 4.7 | 6.5 ± 6.4 | 6.0 ± 7.5 | 2.9 ± 6.6 | 1.4 ± 7.9 | −2.5 ± 10.4* | −1.9 ± 10.0 |
| 10 | 43.7 ± 8.8 | 41.3 ± 10.1 | 41.3 ± 8.2 | 39.4 ± 8.5* | 4.7 ± 3.3 | 3.8 ± 4.9 | 4.4 ± 6.2 | 4.8 ± 7.5 | 4.0 ± 7.1 | 4.5 ± 8.3 | 2.4 ± 11.1 | 2.4 ± 10.6 |
| 20 | 45.4 ± 8.7 | 43.8 ± 9.9 | 43.7 ± 8.3 | 42.8 ± 8.5 | 4.3 ± 3.0 | 3.5 ± 5.5 | 3.8 ± 6.9 | 4.9 ± 7.8 | 4.7 ± 7.4 | 4.7 ± 7.8 | 3.6 ± 10.8 | 3.4 ± 10.2 |
| 30 | 45.7 ± 8.1 | 46.2 ± 10.0 | 46.3 ± 8.6 | 46.6 ± 8.9 | 4.1 ± 2.8 | 1.7 ± 5.2 | 2.3 ± 6.5 | 3.7 ± 7.4 | 4.4 ± 7.7 | 5.3 ± 7.8 | 5.1 ± 11.1 | 4.5 ± 10.5 |
| 40 | 45.3 ± 8.1 | 49.6 ± 10.2* | 49.4 ± 9.2* | 51.8 ± 9.4* | 3.7 ± 3.3 | 0.4 ± 4.9* | 1.6 ± 6.6 | 4.0 ± 7.0 | 4.5 ± 7.8 | 6.2 ± 8.2 | 5.6 ± 11.3 | 4.8 ± 10.4 |
| 50 | 45.0 ± 7.9 | 53.9 ± 10.1* | 52.7 ± 9.3* | 58.0 ± 9.9* | 2.9 ± 3.6 | −1.0 ± 4.8* | 1.6 ± 6.3 | 6.5 ± 7.5 | 5.7 ± 7.3 | 7.2 ± 8.1 | 4.3 ± 10.8 | 4.4 ± 9.9 |
| 60 | 49.9 ± 7.2 | 57.9 ± 9.4* | 56.4 ± 9.0* | 61.7 ± 9.7* | 2.7 ± 3.1 | −1.0 ± 5.6 | 1.9 ± 6 | 7.7 ± 7.6* | 4.6 ± 6.1 | 5.6 ± 7.4 | 2.6 ± 9.8 | 2.9 ± 8.9 |
| 70 | 70.8 ± 8.2 | 72.9 ± 9.0 | 69.6 ± 8.8 | 74.1 ± 9.4* | 1.2 ± 3.5 | −2.8 ± 5.4 | −0.4 ± 6.4 | 6.1 ± 8.3* | 4.9 ± 6.1 | 6.5 ± 6.3 | 7.0 ± 8.7 | 7.8 ± 7.7* |
| 80 | 77.6 ± 11.1 | 72.6 ± 10.7* | 69.8 ± 9.5* | 69.4 ± 9.2* | 0.7 ± 4.1 | −3.4 ± 6.4 | −2.3 ± 7.4 | 1.8 ± 9.0 | 7.2 ± 5.7 | 9.2 ± 6.2 | 8.9 ± 8.6 | 8.3 ± 7.6 |
| 90 | 47.6 ± 8.5 | 41.1 ± 10.2* | 41.7 ± 8.2* | 37.7 ± 8.4* | 3.3 ± 3.7 | 1.6 ± 5.2 | 2.7 ± 6.4 | 5.9 ± 8.2 | 5.9 ± 5.6 | 5.5 ± 6.9 | 3.7 ± 10.6 | 0.8 ± 9.9* |
| 100 | 39.0 ± 7.3 | 36.8 ± 9.2 | 37.2 ± 7.4 | 33.9 ± 7.8* | 4.6 ± 3.8 | 5.2 ± 4.8 | 6.8 ± 6.3 | 6.2 ± 7.5 | 3.1 ± 6.3 | 1.6 ± 7.7 | −2.6 ± 10.0* | −2.0 ± 9.8* |

**Note:**
Means ± standard deviations of stifle flexion/extension, adduction/abduction and internal/external rotation obtained from bone-determined poses (Bone det.) and skin markers with three marker clusters (M1, M2 and M3) during gait. The data points were normalized for a complete gait cycle expressed in percent. The values marked with an asterisk indicates a significant difference ($p < 0.05$) comparing to the bone-determined stifle kinematics.

estimated femoral poses cranially and thus lead to underestimated flexion angles, as indicated by the M1 and M3 clusters (Table 5). The inertial effect of ground contact results in wobbling of the skin and muscle, as reported in a previous human STA study (*Miranda et al., 2013*). However, the soft tissue wobbling following the paw contact, which is possibly present in canine dynamic ambulation, could not be clearly detectable in the present study owing to the limited sampling rate of the fluoroscopic imaging. During the stance phase (0–60% GC), the proximal and cranial displacement of the CT1-3, CLT1-3, LT1-3 and LFC markers and the caudal displacement of the GT marker (Fig. 4B) contributed to a gradually increasing caudal tilt of the femur (Fig. 5C), leading to the overestimation of stifle flexion during 40–60% GC (Table 5). In comparison with the stifle flexion angle during the stance phase (≈11°), the simultaneous hip extension had a slightly greater magnitude (≈16° (*Torres et al., 2013*)), which was expected to considerably impact the movement of thigh markers even though the corresponding parameters were not measurable in the study. During 60–80% GC, the thigh markers moved in the opposite direction as in the stance phase (0–60% GC) by greater distances (Fig. 4D), gradually leading to cranial tilting of the femur (Fig. 5C). These excessive marker displacements might be attributed to the approximately 30° stifle flexion (Fig. 4A), as isolated stifle flexion has been reported to lead to considerable distal displacement of cranial thigh markers in a preceding study conducted on dogs with similar body morphologies (*Lin et al., 2018a*).

The segment pose deviations in dogs were shown to be larger than those reported in a human STA study in terms of the rmsd (*Barre et al., 2013*), especially in the femoral C/C tilt component (Table 4). Other than species-related skin properties (*Bismuth et al., 2014*) that may affect STA amplitudes, since leg length is shorter and thinner in dogs than in humans, the closer intermarker distances in dogs can theoretically yield a higher deviation

of the estimated segment orientation caused by the marker STAs (*Cappozzo et al., 1997*). A similar tendency can also be found when comparing the M1 and M3 clusters (Tables 3 and 4). In addition, 35 markers were used per segment in the study of *Barre et al. (2013)*, which was much more than that used in the current study (i.e., 4 markers) and should have also contributed to the diminished error amplitudes (*Cappozzo et al., 1997*). Observations on the influences of STAs on canine pelvic limb kinematics were made with a 2D kinematics model (*Kim et al., 2011*), in which the stifle angles were derived with and without the assumption of fixed leg length. Even though a direct comparison of the current findings to those of the study by *Kim et al. (2011)* is limited, as the employed kinematic models are different, smaller marker-determined flexion angles of the stifle during the swing phase (80–90% GC) were observed in both studies (Table 5). The overall rmsd in the stifle flexion angle estimation, ranging from 6.2° to 8.7° (Table 4), was also close to the previously reported value of 6.38° (*Kim et al., 2011*).

The rmsd of the femoral I/E rotation reached a maximum of 7.1° during the entire GC (Table 4), comparable to the reported values in human gait (*Barré et al., 2015*; *Barre et al., 2013*), and was most susceptible to the STAs when using the M1 and M2 clusters. *Barre et al. (2013)* and *Reinschmidt et al. (1997)* both reported that during the stance phase, knee I/E rotation was the least accurate component. While the femoral I/E rotation deviation was shown to mostly influence the estimated knee I/E rotation in human gait (*Barré et al., 2015*), this scenario may not be completely applicable to canine gait. During a GC, the stifle joints of dogs are consistently kept in a more flexed position (38.7–80.3°) than those in human gait (1.0–68.6°) (*Gray et al., 2019*), which leads to different propagations of the femoral I/E rotation deviations to the errors of estimated stifle angles between the dog and human. Theoretically, with a certain femoral I/E rotation deviation, increasing the stifle flexion angles would enlarge the Add/Abd errors but diminish the I/E rotation errors of the stifle joint, as the joint coordinate system was applied in the description of joint angles (*Grood & Suntay, 1983*). A similar scenario can be found in *Barré et al. (2015)*, in which the Add/Abd error of the knee is doubled in the swing phase compared to the value in the stance phase, given that the femoral deviations varied below 0.4° for the L/M tilt and I/E rotation components (Table 4) and that flexion angles are considerably higher in the swing phase (*Gray et al., 2019*). Such influences on the estimated stifle angles could also be observed in 40–70% GC, during which an averaged femoral external rotation of 5° (when using the M1 cluster) (Fig. 5B) deteriorated the overestimation of the abduction angle of the stifle joint (Table 5) and vise versa (when using the M3 cluster).

The three marker clusters tested in the current study were not able to accurately reproduce the skeletal kinematics during active ambulation, in which the minimum rmsd of the estimated joint angles of the canine determined from any of the tested marker clusters was 4.5° (Table 4). While the M3 cluster showed the smallest cumulative marker-level STAs, its performance in the determination of stifle angles was not as accurate as expected and not even comparable to that of the M1 and M2 clusters in primary motion component (Tables 4 and 5). The M3 cluster was found to be smaller in

size than the other two clusters (where size is defined as the root-mean-square distance of the markers from their mean position (*Cappozzo et al., 1997*); M1: 70.2 mm; M2: 50.8 mm; M3: 26.9 mm)) and was demonstrated to be more prone to segment pose errors due to the propagation of marker errors (*Cappozzo et al., 1997*). The markers that were distributed concentratedly in a specific region were shown to have relatively similar STAs in magnitudes and directions (Figs. 2 and 3), which may have resulted in the rigid movement of clusters that cannot be addressed with commonly used pose estimators (*Benoit, Damsgaard & Andersen, 2015*). It thus appears that solely choosing markers with smaller STAs was insufficient to ensure an accurate reproduction of the stifle kinematics.
The configuration of the clusters, namely, the number of markers, the geometry characteristics described by the isotropic index, and the size and location of the cluster (*Cappozzo et al., 1997*), should all be taken into account when designing marker clusters. Reproducible marker placement is another prerequisite for reliable kinematic measurements (*Schwencke et al., 2012*). Placing markers on anatomical landmarks near the joint lines, as was done for the M1 cluster, may be advantageous for the repeatability of marker placement (*Torres et al., 2015*) and for larger-sized clusters. However, in accordance with the literature on human STA, attention should also be paid to markers near the joints responsible for movement, as they are normally displaced substantially with respect to the underlying skeletons (*Akbarshahi et al., 2010*; *Cappozzo et al., 1996*; *Peters et al., 2010*; *Sati et al., 1996*; *Tsai et al., 2009*). Comprehensive drawing of the STA magnitude map (*Barré et al., 2015*) on the canine limb with a large number of markers is considered helpful for identifying the proper regions for marker attachment for canine motion analysis.

Kinematic changes associated with joint disorders and treatments are commonly quantified with marker-based motion capture systems (*Böddeker et al., 2012*; *Torres et al., 2017*). For instance, with marker-based gait analysis, *Böddeker et al. (2012)* found that, compared to the preoperative values, the stifle extension angle of cranial cruciate ligament-deficient dogs increased approximately 5° postoperatively throughout the gait cycle. A similar clinical issue was recently investigated with model-based fluoroscopy analysis, which enabled the reporting of the stifle kinematics free from the influence of STAs (*Tinga et al., 2020*). While there must have been some other differences regarding the subjects, surgical details and experimental conditions, etc. between studies, more pronounced flexion angle deviations (approximately 7–20°) in the postoperative stifle joint were observed in *Tinga et al. (2020)*. Although the association between STAs and physical changes related to surgical treatment and recovery is unclear, motion-dependent STA components (e.g., hip, stifle (*Lin et al., 2018a*) and tarsal motion) are likely to increase uncertainty in the quantification of limb function changes considering the magnitudes of and variations in the stifle angle deviation caused by STAs during gait (Tables 4 and 5) and changes in joint motion patterns between pre- and postoperative conditions.

It has been acknowledged that STAs are affected by multiple factors (*Bonci et al., 2014*; *Cappozzo et al., 1996*; *Li et al., 2017*; *Stagni et al., 2005*), including adjacent joint motion, muscle contraction, tendon displacement, and body inertial effects. Examining STAs

during GC could simultaneously involve all of these factors, which could help explain potential errors in marker-based 3D gait analysis, directly contributing to clinical gait analyses and orthopedic examinations. The primary concern of the approach is that the individual effects of each factor on STA behavior are concealed. Factor analysis of various motion tasks comprising different joint activities may help delineate the contributions of each STA factor. The present study recruited Taiwan dogs that were similar in body figure (Table 1) in order to diminish the between-subject variability in the STAs. However, the differences in obesity- and breed-dependent body conformation together with their influences on gait mechanics (*Agostinho et al., 2011*; *Brady et al., 2013*; *Vilar et al., 2016*) indicate that the current findings may not be representative of STA patterns in dogs with dissimilar body morphologies. Studies concentrating on between-breed and between-obesity comparisons of STA patterns may result in a better understanding of the STAs over multiple dog species. Another limitation is related to the limited sampling rate of the data, governed by the current fluoroscopy system (30 fps). High-frequency components of STAs (*Dumas & Jacquelin, 2017*), which may arise from inertial effects during high-speed contact with surrounding objects (e.g., paw contact), were inevitably obscured in the current study.

## CONCLUSIONS

The most prominent marker STAs occurred in the cranial aspect of the thigh during treadmill gait. The crus was less affected by STAs than the thigh. Regardless of the tested marker cluster used, the STAs resulted in orientation deviations from the estimated segment poses, especially in the C/C tilt of the femur and I/E rotation of both segments. The deviated orientations of the segments further led to considerable errors in estimated stifle angles, in which the Flex/Ext and I/E rotation were the most affected kinematic components. In general, the STAs resulted in overestimated flexion angles during the mid-to-terminal stance phase and underestimated flexion angles during the mid-to-terminal swing phases, whereas the selection of marker cluster differently affected the estimated Abd/Add and I/E rotation. Considerable effects of STAs on the marker-based 3D gait analysis of dogs were demonstrated, from which a priori knowledge of STAs and their impacts may help further the development of error-compensation methods.

## ACKNOWLEDGEMENTS

The authors gratefully acknowledge the staff and graduate students of the National Taiwan University Veterinary Hospital for their assistance in the experiments.

## ADDITIONAL INFORMATION AND DECLARATIONS

### Funding

This work was supported by the Ministry of Science and Technology of Taiwan, R.O.C. (grant numbers 107-2311-B-002-017-MY2 and 108-2321-B-197-001). The funders had no role in study design, data collection and analysis, decision to publish, or preparation of the manuscript.

## Grant Disclosures

The following grant information was disclosed by the authors:
Ministry of Science and Technology of Taiwan, R.O.C: 107-2311-B-002-017-MY2 and 108-2321-B-197-001.

## Competing Interests

The authors declare that they have no competing interests.

## Author Contributions

- Cheng-Chung Lin performed the experiments, analyzed the data, prepared figures and/or tables, authored or reviewed drafts of the paper, and approved the final draft.
- Shi-Nuan Wang performed the experiments, analyzed the data, prepared figures and/or tables, and approved the final draft.
- Ming Lu performed the experiments, prepared figures and/or tables, and approved the final draft.
- Tzu-Yi Chao performed the experiments, prepared figures and/or tables, and approved the final draft.
- Tung-Wu Lu conceived and designed the experiments, authored or reviewed drafts of the paper, and approved the final draft.
- Ching-Ho Wu conceived and designed the experiments, authored or reviewed drafts of the paper, and approved the final draft.

## Animal Ethics

The following information was supplied relating to ethical approvals (i.e., approving body and any reference numbers):

The study was approved by the National Taiwan University's Institutional Animal Care and Use Committee (No: NTU106-EL-00221) and the University Hospital's Clinical Trial/Research Committee (Approval No: 000041).

## Data Availability

The following information was supplied regarding data availability:

The raw data of measured marker coordinates and calculated virtual marker coordinates free from the soft tissue artifacts are available in the Supplemental File.

## Supplemental Information

Supplemental information for this article can be found online at http://dx.doi.org/10.7717/peerj.9379#supplemental-information.

# REFERENCES

**Agostinho FS, Rahal SC, Miqueleto NSML, Verdugo MR, Inamassu LR, El-Warrak AO. 2011.** Kinematic analysis of Labrador Retrievers and Rottweilers trotting on a treadmill. *Veterinary and Comparative Orthopaedics and Traumatology* **24(3)**:185–191 DOI 10.3415/VCOT-10-03-0039.

**Akbarshahi M, Schache AG, Fernandez JW, Baker R, Banks S, Pandy MG. 2010.** Non-invasive assessment of soft-tissue artifact and its effect on knee joint kinematics during functional activity. *Journal of Biomechanics* **43(7)**:1292–1301 DOI 10.1016/j.jbiomech.2010.01.002.

**Baltzopoulos V. 1995.** A videofluoroscopy method for optical distortion correction and measurement of knee-joint kinematics. *Clinical Biomechanics* **10(2)**:85–92 DOI 10.1016/0268-0033(95)92044-M.

**Barre A, Thiran JP, Jolles BM, Theumann N, Aminian K. 2013.** Soft tissue artifact assessment during treadmill walking in subjects with total knee arthroplasty. *IEEE Transactions on Biomedical Engineering* **60(11)**:3131–3140 DOI 10.1109/TBME.2013.2268938.

**Barré A, Jolles BM, Theumann N, Aminian K. 2015.** Soft tissue artifact distribution on lower limbs during treadmill gait: influence of skin markers' location on cluster design. *Journal of Biomechanics* **48(10)**:1965–1971 DOI 10.1016/j.jbiomech.2015.04.007.

**Benoit DL, Damsgaard M, Andersen MS. 2015.** Surface marker cluster translation, rotation, scaling and deformation: their contribution to soft tissue artefact and impact on knee joint kinematics. *Journal of Biomechanics* **48(10)**:2124–2129 DOI 10.1016/j.jbiomech.2015.02.050.

**Bismuth C, Gerin C, Viguier E, Fau D, Dupasquier F, Cavetier L, David L, Carozzo C. 2014.** The biomechanical properties of canine skin measured in situ by uniaxial extension. *Journal of Biomechanics* **47(5)**:1067–1073 DOI 10.1016/j.jbiomech.2013.12.027.

**Bockstahler B, Kräutler C, Holler P, Kotschwar A, Vobornik A, Peham C. 2012.** Pelvic limb kinematics and surface electromyography of the vastus lateralis, biceps femoris, and gluteus medius muscle in dogs with hip osteoarthritis. *Veterinary Surgery* **41(1)**:54–62 DOI 10.1111/j.1532-950X.2011.00932.x.

**Bonci T, Camomilla V, Dumas R, Chèze L, Cappozzo A. 2014.** A soft tissue artefact model driven by proximal and distal joint kinematics. *Journal of Biomechanics* **47(10)**:2354–2361 DOI 10.1016/j.jbiomech.2014.04.029.

**Brady RB, Sidiropoulos AN, Bennett HJ, Rider PM, Marcellin-Little DJ, Devita P. 2013.** Evaluation of gait-related variables in lean and obese dogs at a trot. *American Journal of Veterinary Research* **74(5)**:757–762 DOI 10.2460/ajvr.74.5.757.

**Böddeker J, Drüen S, Meyer-Lindenberg A, Fehr M, Nolte I, Wefstaedt P. 2012.** Computer-assisted gait analysis of the dog: comparison of two surgical techniques for the ruptured cranial cruciate ligament. *Veterinary and Comparative Orthopaedics and Traumatology* **25(1)**:11–21 DOI 10.3415/VCOT-10-02-0025.

**Cappello A, Stagni R, Fantozzi S, Leardini A. 2005.** Soft tissue artifact compensation in knee kinematics by double anatomical landmark calibration: performance of a novel method during selected motor tasks. *IEEE Transactions on Biomedical Engineering* **52(6)**:992–998 DOI 10.1109/TBME.2005.846728.

**Cappozzo A, Cappello A, Della Croce U, Pensalfini F. 1997.** Surface-marker cluster design criteria for 3-D bone movement reconstruction. *IEEE Transactions on Biomedical Engineering* **44(12)**:1165–1174 DOI 10.1109/10.649988.

**Cappozzo A, Catani F, Leardini A, Benedetti MG, Della Croce U. 1996.** Position and orientation in space of bones during movement: experimental artefacts. *Clinical Biomechanics* **11(2)**:90–100 DOI 10.1016/0268-0033(95)00046-1.

**Carlisle LD, Memili E, Linford RL, Slater KA, Nicodemus MC. 2019.** Relationship between gait mechanics and the speed of the trot in the Weimaraner dog breed. *Topics in Companion Animal Medicine* **35**:26–30 DOI 10.1053/j.tcam.2019.03.003.

**Cereatti A, Bonci T, Akbarshahi M, Aminian K, Barré A, Begon M, Benoit DL, Charbonnier C, Dal Maso F, Fantozzi S, Lin C-C, Lu T-W, Pandy MG, Stagni R, Van den Bogert AJ,**

**Camomilla V. 2017.** Standardization proposal of soft tissue artefact description for data sharing in human motion measurements. *Journal of Biomechanics* **62**:5–13 DOI 10.1016/j.jbiomech.2017.02.004.

**Chèze L, Fregly BJ, Dimnet J. 1995.** A solidification procedure to facilitate kinematic analyses based on video system data. *Journal of Biomechanics* **28(7)**:879–884 DOI 10.1016/0021-9290(95)95278-D.

**Clément J, De Guise JA, Fuentes A, Hagemeister N. 2018.** Comparison of soft tissue artifact and its effects on knee kinematics between non-obese and obese subjects performing a squatting activity recorded using an exoskeleton. *Gait & Posture* **61**:197–203 DOI 10.1016/j.gaitpost.2018.01.009.

**De Rosario H, Page A, Besa A, Mata V, Conejero E. 2012.** Kinematic description of soft tissue artifacts: quantifying rigid versus deformation components and their relation with bone motion. *Medical & Biological Engineering & Computing* **50(11)**:1173–1181 DOI 10.1007/s11517-012-0978-5.

**Dumas R, Jacquelin E. 2017.** Stiffness of a wobbling mass models analysed by a smooth orthogonal decomposition of the skin movement relative to the underlying bone. *Journal of Biomechanics* **62**:47–52 DOI 10.1016/j.jbiomech.2017.06.002.

**Fischer MS, Lehmann SV, Andrada E. 2018.** Three-dimensional kinematics of canine hind limbs: in vivo, biplanar, high-frequency fluoroscopic analysis of four breeds during walking and trotting. *Scientific Reports* **8(1)**:16982 DOI 10.1038/s41598-018-34310-0.

**Fu Y-C, Torres BT, Budsberg SC. 2010.** Evaluation of a three-dimensional kinematic model for canine gait analysis. *American Journal of Veterinary Research* **71(10)**:1118–1122 DOI 10.2460/ajvr.71.10.1118.

**Gray HA, Guan S, Thomeer LT, Schache AG, De Steiger R, Pandy MG. 2019.** Three-dimensional motion of the knee-joint complex during normal walking revealed by mobile biplane X-ray imaging. *Journal of Orthopaedic Research* **37(3)**:615–630 DOI 10.1002/jor.24226.

**Grimpampi E, Camomilla V, Cereatti A, De Leva P, Cappozzo A. 2014.** Metrics for describing soft-tissue artefact and its effect on pose, size, and shape of marker clusters. *IEEE Transactions on Biomedical Engineering* **61(2)**:362–367 DOI 10.1109/TBME.2013.2279636.

**Grood ES, Suntay WJ. 1983.** A joint coordinate system for the clinical description of three-dimensional motions: application to the knee. *Journal of Biomechanical Engineering* **105(2)**:136–144 DOI 10.1115/1.3138397.

**Hume DR, Kefala V, Harris MD, Shelburne KB. 2018.** Comparison of marker-based and stereo radiography knee kinematics in activities of daily living. *Annals of Biomedical Engineering* **46(11)**:1806–1815 DOI 10.1007/s10439-018-2068-9.

**Jones SC, Kim SE, Banks SA, Conrad BP, Abbasi AZ, Tremolada G, Lewis DD, Pozzi A. 2014.** Accuracy of noninvasive, single-plane fluoroscopic analysis for measurement of three-dimensional femorotibial joint poses in dogs. *American Journal of Veterinary Research* **75(5)**:477–485 DOI 10.2460/ajvr.75.5.477.

**Kim SE, Jones SC, Lewis DD, Banks SA, Conrad BP, Tremolada G, Abbasi AZ, Coggeshall JD, Pozzi A. 2015.** In-vivo three-dimensional knee kinematics during daily activities in dogs. *Journal of Orthopaedic Research* **33(11)**:1603–1610 DOI 10.1002/jor.22927.

**Kim SY, Kim JY, Hayashi K, Kapatkin AS. 2011.** Skin movement during the kinematic analysis of the canine pelvic limb. *Veterinary and Comparative Orthopaedics and Traumatology* **24(5)**:326–332 DOI 10.3415/VCOT-10-08-0123.

**Kim J, Rietdyk S, Breur GJ. 2008.** Comparison of two-dimensional and three-dimensional systems for kinematic analysis of the sagittal motion of canine hind limbs during walking. *American Journal of Veterinary Research* **69(9)**:1116–1122 DOI 10.2460/ajvr.69.9.1116.

**Kuo MY, Tsai TY, Lin CC, Lu TW, Hsu HC, Shen WC. 2011.** Influence of soft tissue artifacts on the calculated kinematics and kinetics of total knee replacements during sit-to-stand. *Gait and Posture* **33(3)**:379–384 DOI 10.1016/j.gaitpost.2010.12.007.

**Laflamme D. 1997.** Development and validation of a body condition score system for dogs. *Canine practice* **22**:10–15.

**Leardini A, Chiari L, Della Croce U, Cappozzo A. 2005.** Human movement analysis using stereophotogrammetry—Part 3: soft tissue artifact assessment and compensation. *Gait & Posture* **21(2)**:212–225 DOI 10.1016/j.gaitpost.2004.05.002.

**Li J-D, Lu T-W, Lin C-C, Kuo M-Y, Hsu H-C, Shen W-C. 2017.** Soft tissue artefacts of skin markers on the lower limb during cycling: effects of joint angles and pedal resistance. *Journal of Biomechanics* **62**:27–38 DOI 10.1016/j.jbiomech.2017.03.018.

**Li K, Zheng L, Tashman S, Zhang X. 2012.** The inaccuracy of surface-measured model-derived tibiofemoral kinematics. *Journal of Biomechanics* **45(15)**:2719–2723 DOI 10.1016/j.jbiomech.2012.08.007.

**Lin C-C, Chang C-L, Lu M, Lu T-W, Wu C-H. 2018a.** Quantification of three-dimensional soft tissue artifacts in the canine hindlimb during passive stifle motion. *BMC Veterinary Research* **14(1)**:389 DOI 10.1186/s12917-018-1714-7.

**Lin C-C, Li J-D, Lu T-W, Kuo M-Y, Kuo C-C, Hsu H-C. 2018b.** A model-based tracking method for measuring 3D dynamic joint motion using an alternating biplane x-ray imaging system. *Medical Physics* **45(8)**:3637–3649 DOI 10.1002/mp.13042.

**Lin C-C, Lu T-W, Lu H-L, Kuo M-Y, Hsu H-C. 2016.** Effects of soft tissue artifacts on differentiating kinematic differences between natural and replaced knee joints during functional activity. *Gait & Posture* **46**:154–160 DOI 10.1016/j.gaitpost.2016.03.006.

**Lin C-C, Lu T-W, Shih T-F, Tsai T-Y, Wang T-M, Hsu S-J. 2013.** Intervertebral anticollision constraints improve out-of-plane translation accuracy of a single-plane fluoroscopy-to-CT registration method for measuring spinal motion. *Medical Physics* **40(3)**:031912 DOI 10.1118/1.4792309.

**Lorensen WE, Cline HE. 1987.** Marching cubes: a high resolution 3D surface construction algorithm. *Computer Graphics (ACM)* **21(4)**:163–169 DOI 10.1145/37402.37422.

**Lorke M, Willen M, Lucas K, Beyerbach M, Wefstaedt P, Murua Escobar H, Nolte I. 2017.** Comparative kinematic gait analysis in young and old Beagle dogs. *Journal of Veterinary Science* **18(4)**:521–530 DOI 10.4142/jvs.2017.18.4.521.

**Lu M, Lin C-C, Lu T-W, Wang S-N, Wu C-H. 2020.** Effects of soft tissue artefacts on computed segmental and stifle kinematics in canine motion analysis. *Veterinary Record* **86(2)**:66 DOI 10.1136/vr.105352.

**Lu TW, O'Connor JJ. 1999.** Bone position estimation from skin marker co-ordinates using global optimisation with joint constraints. *Journal of Biomechanics* **32(2)**:129–134 DOI 10.1016/S0021-9290(98)00158-4.

**Miranda DL, Rainbow MJ, Crisco JJ, Fleming BC. 2013.** Kinematic differences between optical motion capture and biplanar videoradiography during a jump-cut maneuver. *Journal of Biomechanics* **46(3)**:567–573 DOI 10.1016/j.jbiomech.2012.09.023.

**Peters A, Galna B, Sangeux M, Morris M, Baker R. 2010.** Quantification of soft tissue artifact in lower limb human motion analysis: A systematic review. *Gait & Posture* **31(1)**:1–8 DOI 10.1016/j.gaitpost.2009.09.004.

**Piazza AM, Binversie EE, Baker LA, Nemke B, Sample SJ, Muir P. 2017.** Variance associated with walking velocity during force platform gait analysis of a heterogeneous sample of clinically normal dogs. *American Journal of Veterinary Research* **78(4)**:500–507 DOI 10.2460/ajvr.78.4.500.

**Rafael C, Gonzalez REW. 2017.** *Digital image processing*. London: Pearson Education Limited.

**Reinschmidt C, Van den Bogert AJ, Lundberg A, Nigg BM, Murphy N, Stacoff A, Stano A. 1997.** Tibiofemoral and tibiocalcaneal motion during walking: external vs. skeletal markers. *Gait & Posture* **6(2)**:98–109 DOI 10.1016/S0966-6362(97)01110-7.

**Richard V, Cappozzo A, Dumas R. 2017.** Comparative assessment of knee joint models used in multi-body kinematics optimisation for soft tissue artefact compensation. *Journal of Biomechanics* **62**:95–101 DOI 10.1016/j.jbiomech.2017.01.030.

**Sanchez-Bustinduy M, De Medeiros MA, Radke H, Langley-Hobbs S, McKinley T, Jeffery N. 2010.** Comparison of kinematic variables in defining lameness caused by naturally occurring rupture of the cranial cruciate ligament in dogs. *Veterinary Surgery* **39(4)**:523–530 DOI 10.1111/j.1532-950X.2010.00672.x.

**Sati M, De Guise JA, Larouche S, Drouin G. 1996.** Quantitative assessment of skin-bone movement at the knee. *Knee* **3(3)**:121–138 DOI 10.1016/0968-0160(96)00210-4.

**Schwencke M, Smolders LA, Bergknut N, Gustås P, Meij BP, Hazewinkel HA. 2012.** Soft tissue artifact in canine kinematic gait analysis. *Veterinary Surgery* **41(7)**:829–837 DOI 10.1111/j.1532-950X.2012.01021.x.

**Smith TJ, Baltzer WI, Jelinski SE, Salinardi BJ. 2013.** Inter- and intratester reliability of anthropometric assessment of limb circumference in labrador retrievers. *Veterinary Surgery* **42(3)**:316–321 DOI 10.1111/j.1532-950X.2013.01102.x.

**Stagni R, Fantozzi S, Cappello A, Leardini A. 2005.** Quantification of soft tissue artefact in motion analysis by combining 3D fluoroscopy and stereophotogrammetry: a study on two subjects. *Clinical Biomechanics* **20(3)**:320–329 DOI 10.1016/j.clinbiomech.2004.11.012.

**Söderkvist I, Wedin P-Å. 1993.** Determining the movements of the skeleton using well-configured markers. *Journal of Biomechanics* **26(12)**:1473–1477 DOI 10.1016/0021-9290(93)90098-Y.

**Taylor WR, Ehrig RM, Duda GN, Schell H, Seebeck P, Heller MO. 2005.** On the influence of soft tissue coverage in the determination of bone kinematics using skin markers. *Journal of Orthopaedic Research* **23(4)**:726–734 DOI 10.1016/j.orthres.2005.02.006.

**Tinga S, Kim SE, Banks SA, Jones SC, Park BH, Burtch M, Pozzi A, Lewis DD. 2020.** Femorotibial kinematics in dogs treated with tibial plateau leveling osteotomy for cranial cruciate ligament insufficiency: an in vivo fluoroscopic analysis during walking. *Veterinary Surgery* **49**:187–199 DOI 10.1111/vsu.13356.

**Torres BT, Fu Y-C, Sandberg GS, Budsberg SC. 2017.** Pelvic limb kinematics in the dog with and without a stifle orthosis. *Veterinary Surgery* **46(5)**:642–652 DOI 10.1111/vsu.12634.

**Torres BT, Gilbert PJ, Reynolds LR, Fu Y-C, Navik JA, Sornborger A, Budsberg SC. 2015.** The effect of examiner variability on multiple canine stifle kinematic gait collections in a 3-dimensional model. *Veterinary Surgery* **44(5)**:581–587 DOI 10.1111/j.1532-950X.2014.12311.x.

**Torres BT, Moëns NMM, Al-Nadaf S, Reynolds LR, Fu Y-C, Budsberg SC. 2013.** Comparison of overground and treadmill-based gaits of dogs. *American Journal of Veterinary Research* **74(4)**:535–541 DOI 10.2460/ajvr.74.4.535.

**Tsai TY, Lu TW, Kuo MY, Hsu HC. 2009.** Quantification of three-dimensional movement of skin markers relative to the underlying bones during functional activities. *Biomedical Engineering: Applications, Basis and Communications* **21(3)**:223–232 DOI 10.4015/S1016237209001283.

**Tsai TY, Lu TW, Kuo MY, Lin CC. 2011.** Effects of soft tissue artifacts on the calculated kinematics and kinetics of the knee during stair-ascent. *Journal of Biomechanics* **44(6)**:1182–1188 DOI 10.1016/j.jbiomech.2011.01.009.

**Vilar JM, Rubio M, Carrillo JM, Domínguez AM, Mitat A, Batista M. 2016.** Biomechanic characteristics of gait of four breeds of dogs with different conformations at walk on a treadmill. *Journal of Applied Animal Research* **44(1)**:252–257 DOI 10.1080/09712119.2015.1031778.

**Wu G, Cavanagh PR. 1995.** ISB recommendations for standardization in the reporting of kinematic data. *Journal of Biomechanics* **28(10)**:1257–1261 DOI 10.1016/0021-9290(95)00017-C.